

Geophysical Research Letters

RESEARCH LETTER

10.1029/2019GL086040

Key Points:

- Near the dawnside, energy-dispersively injected electrons generated plasmaspheric hiss with globally drifting frequencies
- The frequency drift feature allowed tracing the plasmaspheric hiss propagation from the dawnside to the noonside
- The dayside plasmaspheric hiss dissipated away roughly within a magnetic local time span of 5 hr

Supporting Information:

- Supporting Information S1

Correspondence to:

Z. Su,
szpe@mail.ustc.edu.cn

Citation:

Liu, N., Su, Z., Gao, Z., Zheng, H., Wang, Y., Wang, S. et al. (2020). Comprehensive observations of substorm-enhanced plasmaspheric hiss generation, propagation, and dissipation. *Geophysical Research Letters*, 47, e2019GL086040. <https://doi.org/10.1029/2019GL086040>

Received 29 OCT 2019

Accepted 5 JAN 2020

Accepted article online 13 JAN 2020

Comprehensive Observations of Substorm-Enhanced Plasmaspheric Hiss Generation, Propagation, and Dissipation

Nigang Liu^{1,2,3}, **Zhenpeng Su**^{1,2}, **Zhonglei Gao**^{4,5}, **Huinan Zheng**^{1,2}, **Yuming Wang**^{1,2},
Shui Wang^{1,2}, **Yoshizumi Miyoshi**⁶, **Iku Shinohara**⁷, **Yoshiya Kasahara**⁸, **Fuminori Tsuchiya**⁹,
Atsushi Kumamoto⁹, **Shoya Matsuda**⁷, **Masafumi Shoji**⁶, **Takefumi Mitani**⁷, **Takeshi Takashima**⁷,
Yoichi Kazama¹⁰, **Bo-Jhou Wang**¹⁰, **Shiang-Yu Wang**¹⁰, **Chae-Woo Jun**⁶, **Tzu-Fang Chang**¹¹,
Sunny W. Y. Tam¹¹, **Satoshi Kasahara**¹², **Shoichiro Yokota**¹³, **Kunihiro Keika**¹², **Tomoaki Hori**⁶,
 and **Ayako Matsuoka**⁷

¹CAS Key Laboratory of Geospace Environment, Department of Geophysics and Planetary Sciences, University of Science and Technology of China, Hefei, China, ²CAS Center for Excellence in Comparative Planetology, University of Science and Technology of China, Hefei, China, ³Mengcheng National Geophysical Observatory, School of Earth and Space Sciences, University of Science and Technology of China, Hefei, China, ⁴Institute of Space Science and Applied Technology, Harbin Institute of Technology, Shenzhen, China, ⁵School of Physics and Electronic Sciences, Changsha University of Science and Technology, Changsha, China, ⁶Institute for Space-Earth Environmental Research, Nagoya University, Nagoya, Japan, ⁷Institute of Space and Astronautical Science, Japan Aerospace Exploration Agency, Kanagawa, Japan, ⁸Graduate School of Natural Science and Technology, Kanazawa University, Kanazawa, Japan, ⁹Graduate School of Science, Tohoku University, Sendai, Japan, ¹⁰Academia Sinica Institute of Astronomy and Astrophysics, Taipei, Taiwan, ¹¹Institute of Space and Plasma Sciences, National Cheng Kung University, Tainan, Taiwan, ¹²Graduate School of Science, University of Tokyo, Tokyo, Japan, ¹³Graduate School of Science, Osaka University, Osaka, Japan

Abstract Plasmaspheric hiss is an important whistler-mode emission shaping the Van Allen radiation belt environment. How the plasmaspheric hiss waves are generated, propagate, and dissipate remains under intense debate. With the five spacecraft of Van Allen Probes, Exploration of energization and Radiation in Geospace (Arase), and Geostationary Operational Environmental Satellites missions at widely spaced locations, we present here the first comprehensive observations of hiss waves growing from the substorm-injected electron instability, spreading within the plasmasphere, and dissipating over a large spatial scale. During substorms, hot electrons were injected energy-dispersively into the plasmasphere near the dawnside and, probably through a combination of linear and nonlinear cyclotron resonances, generated whistler-mode waves with globally drifting frequencies. These waves were able to propagate from the dawnside to the noonside, with the frequency-drifting feature retained. Approximately 5 hr of magnetic local time away from the source region in the dayside sector, the wave power was dissipated to e^{-4} of its original level.

Plain Language Summary A noisy band of electromagnetic waves with frequencies ranging from tens of hertz to several kilohertz in the Earth's plasmasphere is termed plasmaspheric hiss. These waves are recognized to shape the Van Allen radiation belt environment and then affect the spacecraft survivability and lifetime. How the plasmaspheric hiss waves are generated, propagate, and dissipate has been a fundamental unanswered question since their discovery. With three space missions scattered in the inner magnetosphere, we present here the first comprehensive observations of hiss waves growing from the substorm-injected electron instability, spreading within the plasmasphere, and dissipating over a large spatial scale. These findings have significant implications for the modeling of the plasmaspheric hiss waves and the Van Allen radiation belt dynamics.

1. Introduction

Plasmaspheric hiss waves have long been recognized to shape the Earth's radiation belt environment (Breneman et al., 2015; Mourenas et al., 2017; Lyons et al., 1972; Summers et al., 2007; Thorne et al., 2013). They occur characteristically in the high-density plasmaspheric body and plume with a strong day-night

asymmetry (Li et al., 2015; Meredith et al., 2004; Summers et al., 2008; Thorne et al., 1973; Tsurutani et al., 2015). These waves persist with an amplitude of 10 pT or less during quiescent times (Tsurutani et al., 1975) and intensify to an amplitude of a few hundred picotesla or even several nanotesla during substorms (Meredith et al., 2004; Su et al., 2018a, 2018b). In the frequency-time spectrogram, the hiss waves usually appear as a noisy band from tens of hertz to several kilohertz (Li et al., 2013; Russell et al., 1969; Thorne et al., 1973). Recently, the noisy band has been interpreted as a superposition of random falling and rising tones on a timescale of 0.01 s (Nakamura et al., 2016, 2018; Summers et al., 2014).

How the plasmaspheric hiss waves are generated, propagate, and dissipate remains under active debate. Since their discovery, two competing scenarios have been proposed. One of them postulates linear or non-linear amplification of ambient electromagnetic noise to hiss by unstable hot electrons in the plasmasphere (Omura et al., 2015; Thorne et al., 1979), and the other envisions the entry of lightning-associated whistlers (Green et al., 2005; Sonwalkar & Inan, 1989) or plasmatrough chorus (Bortnik et al., 2008, 2009; Church & Thorne, 1983) to the plasmasphere for further amplification. Both scenarios involve the propagation and dissipation of waves to produce uneven distribution of wave power inside the plasmasphere (Chen et al., 2009, 2014; Church & Thorne, 1983; Chum & Santolík, 2005). In contrast to numerous observational and numerical evidences for the latter scenario linking hiss to chorus (Agapitov et al., 2018; Bortnik et al., 2008, 2009; Chen et al., 2009, 2012; Li et al., 2015, 2017; Malaspina et al., 2016; Su et al., 2015; Tsurutani et al., 2012), the importance of the former scenario has not been determined definitely (Laakso et al., 2015; Meredith et al., 2006, 2018; Tsurutani et al., 2015) because of the challenging requirements on spacecraft locations and data processing techniques. Multiple spacecraft are required to simultaneously measure hiss waves: one monitoring the wave source and the others scattered throughout the plasmasphere detecting the propagating and dissipating waves. Most of the time, the high-resolution wave data are unavailable, not conducive to inter-comparing waves between different spacecraft. New techniques are required to operate on the low-resolution data in order to identify a “marker” for the link between hiss waves over a broad spatial range inside the plasmasphere.

In this letter, we show the first comprehensive measurements of internal generation, three-dimensional propagation, and integrated dissipation of plasmaspheric hiss during substorms, made with the Van Allen Probes (Mauk et al., 2013), the Exploration of energization and Radiation in Geospace (ERG, nicknamed Arase) spacecraft (Miyoshi et al., 2018), and the Geostationary Operational Environmental Satellites (GOES; Davis, 2007). Inside the plasmasphere, the substorm-injected, energy-dispersive electrons generated hiss waves with globally drifting frequencies on a timescale of 1 hr. This frequency drift feature allowed us to trace the propagation of hiss waves over a large spatial scale and then estimate their integrated dissipation.

2. Data and Method

The Van Allen Probes mission contained two identically instrumented probes in nearly the same orbits. We use the data from the Electric and Magnetic Field Instrument and Integrated Science suite (Kletzing et al., 2013) and the Helium Oxygen Proton Electron Mass Spectrometer (Funsten et al., 2013) and the Magnetic Electron Ion Spectrometer (Blake et al., 2013) of the Energetic particle, Composition and the Thermal plasma suite (Spence et al., 2013) on board the Van Allen Probes mission. For the ERG spacecraft (Miyoshi et al., 2018), we use the data from the Onboard Frequency Analyzer (Matsuda et al., 2018) and the High Frequency Analyzer (Kumamoto et al., 2018) of the Plasma Wave Experiment (Kasahara et al., 2018), the Magnetic Field Experiment (Matsuoka et al., 2018), the Low-energy Particle Experiments-electron Analyzer (Kazama et al., 2017), the Medium-energy Particle Experiments-electron Analyzer (Kasahara et al., 2018), and the High-energy Electron Experiment (Mitani et al., 2018). For the GOES mission, GOES-14 and GOES-15 spacecraft were operating at 105° and 135° geographic west longitude, and we use only the data from the Magnetospheric Electron Detector (GOES N Series Data Book, 2009).

For the Van Allen Probes, the electric field measurements along the spacecraft axis are contaminated by the antenna sheath impedance (Hartley et al., 2016). To avoid the electric field contamination, we estimate the wave vector direction and polarization characteristics by applying the singular value decomposition technique (Santolík et al., 2002, 2003) on the wave magnetic spectral matrices. This method allows a 180° ambiguity in the wave vector direction. It is expedient to estimate the signs of the field-aligned Poynting fluxes of waves from the cross-power spectra between the components of electric and magnetic fields (Santolík et al., 2010). Particularly, for the low-frequency (< 1 kHz) waves in the high-density (> 20 cm $^{-3}$)

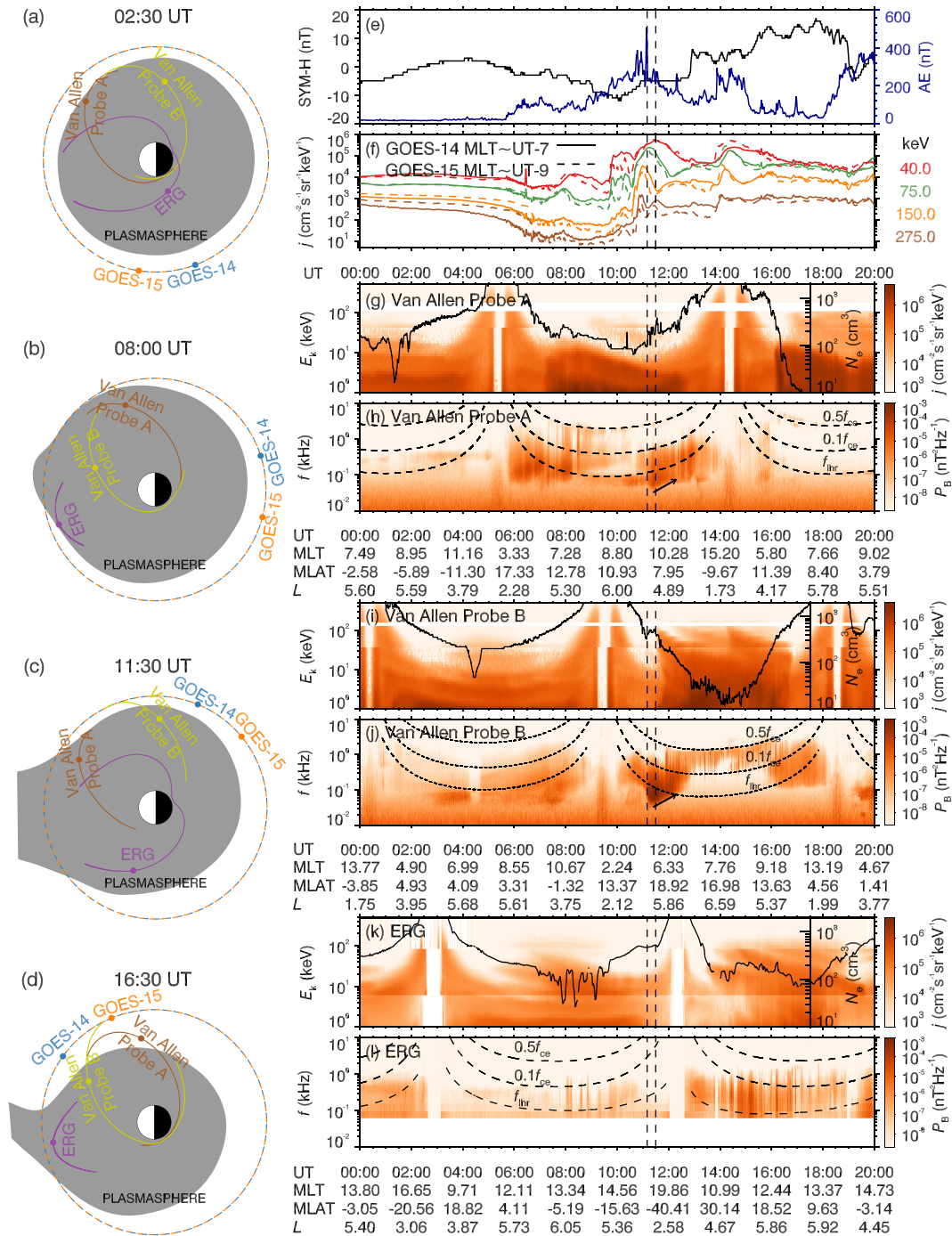


Figure 1. Overview of the 13 January 2018 plasmaspheric hiss event. (a–d) Schematic diagrams of plasmasphere structures (shadows) and spacecraft locations (colored dots) at 02:30, 08:00, 11:30, and 16:40 UT, respectively. The plasmasphere shadows are illustrative cartoons based on the density profiles of the Van Allen Probes and ERG missions, whose trajectories (solid lines) covered the period 00:00–05:30, 05:30–10:00, 10:00–14:00, and 14:00–20:00 UT in Figures 1a–1d, respectively. (e) Geomagnetic activity indices SYM-H and AE. (f) Hot electron differential flux profiles j . (g, i, k) Hot electron differential energy spectra j , with the overplotted local electron densities N_e . (h, j, l) Wave magnetic power spectra P_B , with the overplotted frequencies $0.5 f_{ce}$, $0.1 f_{ce}$, and f_{lhr} . f_{ce} is the equatorial electron gyrofrequency, and f_{lhr} is the equatorial lower hybrid resonance frequency. The vertical dashed lines mark the sudden enhancement of hiss waves and the substorm injection front observed by Van Allen Probe B, respectively. The blank region represents the data gap.

region, the instrument-plasma coupling effect may be relatively limited (Figure 4a of Hartley et al., 2016). The growth rates of inner magnetospheric whistler-mode waves usually peak at the equator. We calculate the linear growth rates (Kenne, 1966) of parallel-propagating whistler-mode waves at the equator using our previously developed code (Liu et al., 2018, 2018; Su et al., 2018a). The equatorial magnetic field can be estimated from the modeled ratio between equatorial and local magnetic fields (Tsyganenko & Sitnov, 2005). The equatorial electron density is modeled as (Denton et al., 2002) $N_{eq} = N_e(\cos \lambda)^{2v}$, where N_e is local electron density derived from the upper hybrid resonance frequency (Kumamoto et al., 2018; Kurth et al., 2014; Matsuoka et al., 2018), λ is the magnetic latitude of the spacecraft, and $v = 3$ (Denton et al., 2002) characterizes the latitudinal variation of density on the downside. To allow the instability calculation, the equatorial distribution of 0.1–300 keV electrons is expediently set to be the same as the observed local distribution.

3. Event Overview

Figure 1 gives an overview of the 13 January 2018 event. Throughout the plotted time period, the magnetosphere was free from storms (with the SYM-H minima of -13 nT). Before 05:30 UT, there was no substorm ($AE < 30$ nT), and Van Allen Probes and ERG observed quite weak ($P_B \sim 3 \times 10^{-7}$ nT 2 /Hz) hiss waves in the expanded dayside plasmasphere $L \sim < 6.0$ (Figure 1a). Note that L is defined as the geocentric equatorial distance of the magnetic field line in the geomagnetic model of Tsyganenko and Sitnov (2005). In the next 4 hr, the weak substorms ($AE < 150$ nT) injected hot electrons to the relatively large L shells ($L \sim 5.5$), which were detected by GOES-14, GOES-15, and Van Allen Probe A in the midnight-dawn-noon sector (Figure 1b). The enhanced plasmaspheric hiss exhibited a strong asymmetry in magnetic local time (MLT). Within the spacecraft orbital coverage, the plasmaspheric hiss power peaked ($P_B \sim 5 \times 10^{-5}$ nT 2 /Hz) on the downside (Van Allen Probe A), followed by about an order-of-magnitude decrease on the noonside (Van Allen Probe B), and almost disappeared on the afternoonside (ERG). With the strong substorms (AE maxima of 500 nT) around 11:00 UT (Figures 1c), GOES-14 and GOES-15 encountered the substorm injection of electrons in the predawn sector, Van Allen Probe B detected the enhancement of hot electrons and hiss waves ($P_B \sim 10^{-3}$ nT 2 /Hz) near the downside, Van Allen Probe A received the hiss waves with lower intensities in the absence of electron injection close to the noonside, and ERG observed neither electron injection nor hiss waves inside the plasmasphere on the duskside. Interestingly, the plasmaspheric hiss observed by Van Allen Probes A and B had frequencies drifting slowly with time, whose lower cutoff (marked by the arrows in Figures 1h and 1j) increased from ~ 30 to ~ 100 Hz on a timescale of 1 hr. We will focus on the generation, propagation, and dissipation of these intense, frequency-drifting plasmaspheric hiss in this letter. After 14:00 UT, the plasmasphere had eroded substantially (Figure 1d). In the noonside plasmaspheric plume, ERG detected the injection of hot electrons and the enhanced hiss waves. In the prenoon sector, there were moderate plasmaspheric hiss waves (Van Allen Probe B) but intermittent and weak plasmatrough chorus waves (Van Allen Probe A).

4. Frequency-Drifting Hiss Generation

In Figures 2a–2f, we evaluate the potential contribution of linear instability of hot (0.1–300 keV) electrons to the whistler-mode waves observed by Van Allen Probe B during 11:30–14:00 UT. These whistler-mode waves with ellipticity $E_B > 0.5$ are identified as hiss waves in the high-density plasmasphere (before 12:50 UT) and chorus waves in the low-density plasmatrough (after 12:50 UT). Before 11:40 UT, the equatorial linear instability is unable to explain the occurrence of plasmaspheric hiss waves. The calculated linear instabilities of hot electrons allow only weak growth ($K_i < 5 \times 10^{-8}$ m $^{-1}$) or even damping ($K_i < 0$) of whistler-mode waves. The core part of hiss waves exhibited bidirectional Poynting fluxes $S_B = \pm 1$ and random wave normal angles $\psi_B \sim 30\text{--}70^\circ$ or $110\text{--}150^\circ$, which must originate from other regions. During 11:40–12:50 UT, the observed hiss waves had poleward Poynting fluxes and quasi-field-aligned wave vectors in the frequency range 70–2,000 Hz, whose source region was likely located near the equator. The injection of hot electrons causes the linear growth rates to increase to a high level ($K_i \sim 3 \times 10^{-7}$ m $^{-1}$), and the linear instability frequency range (< 700 Hz) agrees with the frequency range of the intense hiss waves. At higher frequencies (> 700 Hz), additional physical processes, for example, nonlinear processes (Omura et al., 2015), are required to explain the generation of waves. According to the cyclotron resonant condition, the lower-energy electrons can resonate with the higher-frequency waves. The energy-dispersive injection of hot electrons naturally accounted for the global drift of hiss waves in frequency. Considering that the substorm-enhanced

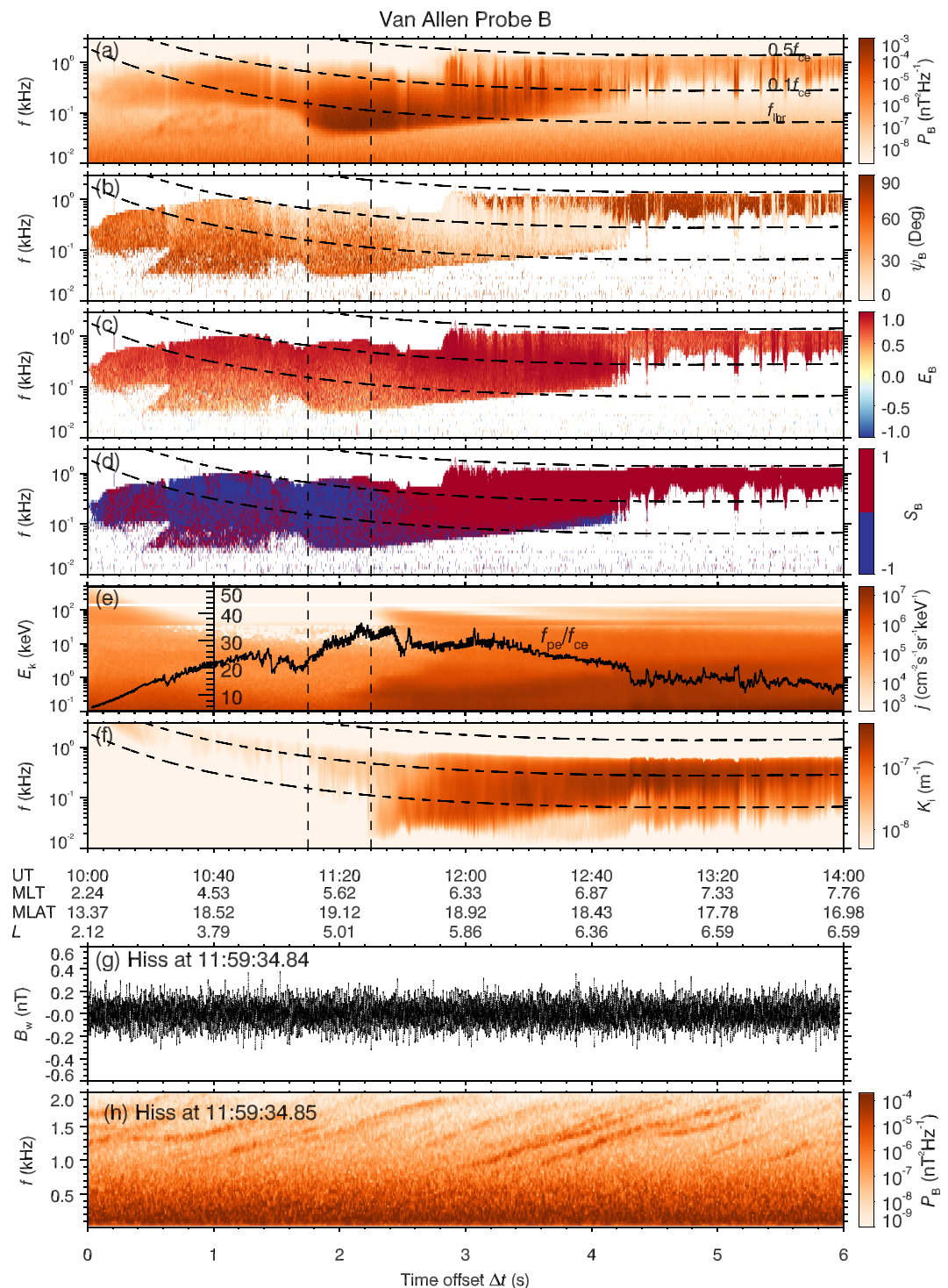


Figure 2. Magnetospheric wave instability during 10:00–14:00 UT: (a) wave magnetic power spectra P_B ; (b) wave normal angles ψ_B (with a 180° ambiguity); (c) ellipticities E_B (negative for left-handed polarized waves and positive for right-handed ones); (d) wave parallel Poynting flux signs S_B (positive for parallel flowing and negative for antiparallel flowing); (e) hot electron differential energy spectra j , with the overplotted equatorial ratio between electron plasma frequency and cyclotron frequency f_{pe}/f_{ce} ; (f) linear spatial growth rates K_i of parallel-propagating whistler-mode waves; (g) burst-mode waveform B_w ; (h) burst-mode magnetic power spectra P_B . The vertical dashed lines in Figures 2a–2f mark the sudden enhancement of hiss waves and substorm injection front observed by Van Allen Probe B, respectively.

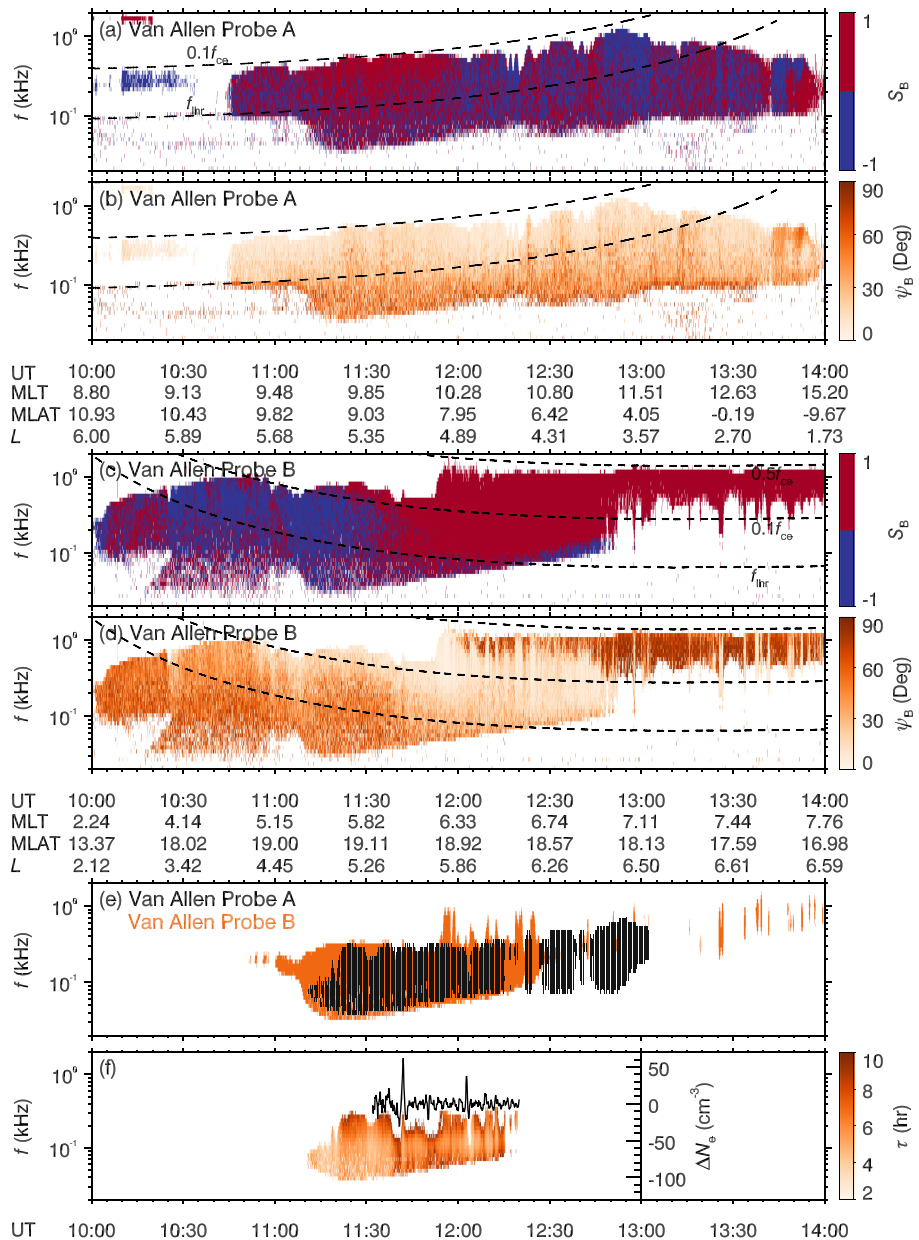


Figure 3. Intercomparing waves between Van Allen Probes A and B during 10:00–14:00 UT: (a, c) parallel Poynting flux signs S_B and (b, d) normal angles ψ_B of righthand-polarized waves ($E_B > 0.5$); (e) isolated intense signals $P_B > 3.0 \times 10^{-6} \text{ nT}^2/\text{Hz}$ for Van Allen Probe A (gray) and $P_B > 1.0 \times 10^{-5} \text{ nT}^2/\text{Hz}$ for Van Allen Probe B (red); (f) wave effective MLT coverage τ , with the overplotted local density fluctuation ΔN_e of Van Allen Probe B. ΔN_e is defined as a 32 s running average minus a 135 s running average of N_e .

waves exhibited a steady increasing trend in frequency approximately from 11:10 to 12:50 UT, we speculate that the enhanced hiss waves before 11:40 UT were still generated inside the plasmasphere and their source region was probably located at a MLT smaller than that of Van Allen Probe B. This speculation is supported by the relative timing of the sudden hiss enhancement near the dawnside (Van Allen Probe B) and the substorm injection of hot electrons in the predawn sector (GOES-14 and GOES-15). After 12:50 UT, chorus waves were clearly modulated by the background density. The corresponding linear instability is restricted within a lower frequency range than the observed chorus waves. This disagreement may be partially attributed to the underestimation of equatorial electron temperature anisotropy with measurements at midlatitudes of $\sim 18^\circ$.

The linear growth rates (Figure 2f) appear to be insufficient to explain the large amplitudes (up to 0.4 nT, as shown in Figure 2g) and the high-frequency extension (up to $\sim 2,000$ Hz) of hiss waves. In the burst frequency-time spectrogram (Figure 2h), there were rising tones extending from 0.7 to 2.0 kHz with lifetimes of ~ 1 s, demonstrating the contribution of nonlinear processes (Omura et al., 2008, 2015). The nonlinear resonant processes tend to produce discrete frequency-time elements with shorter lifetimes at lower frequencies (Nakamura et al., 2016; Omura et al., 2015). The noisy band below 0.7 kHz might be interpreted as a superposition of random falling and rising tones with lifetimes of ~ 0.01 s (Summers et al., 2014). After the initial linear instabilities, the subsequent nonlinear resonant processes could rapidly amplify waves to high intensities and simultaneously make waves extend beyond the linear growth frequency range (Omura et al., 2015). Similar physical processes (Omura et al., 2008) might also affect the frequency dependence of plasmatrough chorus waves.

5. Frequency-Drifting Hiss Propagation and Dissipation

In Figures 3a–3e, we compare the large-scale wave characteristics of Van Allen Probes A and B separated in MLT by ~ 4 hr. From 11:10 to 12:20 UT, Van Allen Probes A and B simultaneously detected the similar frequency-drifting hiss on their inbound and outbound passes, implying that the frequency drift was not a manifestation of the spatial dependence of waves but a temporal behavior of waves over a broad spatial scale. Throughout the time of interest, the lower cutoff frequencies of hiss waves at the two spacecraft always agreed well with each other, and their upper cutoff frequencies, which were strongly modulated by the background densities, still exhibited a certain agreement. These observations demonstrate the close relationship between the core parts (~ 30 –300 Hz) of hiss waves over a broad MLT span. Note that the high-frequency (> 300 Hz) waves had a too weak power to be traced far away from the source. Before 11:40 UT, hiss waves of both spacecraft exhibited bidirectional Poynting fluxes and oblique wave normal angles, whose source region was likely located at a smaller MLT than Van Allen Probe B inside the plasmasphere. After 11:40 UT, the injected electrons drifted to Van Allen Probe B near the dawnside and generated hiss waves propagating away from the equator. After multiple bounces in the plasmasphere, these hiss waves likely reached Van Allen Probe A and exhibited the same frequency drift feature. The hiss waves at Van Allen Probe A tended to have larger normal angles (particularly below 200 Hz) than those at Van Allen Probe B, and the large normal angles may favor the Landau damping of waves during propagation. Meanwhile, part of hiss waves could leak through the high-latitude plasmapause (Bortnik et al., 2008; Liu et al., 2019; Zhu et al., 2015), serving as an additional dissipation process.

In the linear theory, the evolution of wave amplitude B_w can be written as (e.g., Horne, 1989)

$$B_w(s) = B_w(s_0) \exp \left(\int_{s_0}^s K_i ds \right), \quad (1)$$

with the spatial growth rate K_i and the propagation path s . Imitating the above definition, we assume that the wave power $P_B \propto B_w^2$ varies in the following form during propagation from the initial MLT_0 to an arbitrary MLT

$$P_B(MLT, f) = P_B(MLT_0, f) \left[\exp \left(-2 \frac{MLT - MLT_0}{\tau(f)} \right) \right]^2. \quad (2)$$

with $2/\tau$ interpreted as the equivalent spatial dissipation rate and τ termed the wave effective MLT coverage. When the waves propagate away from the source by $\Delta MLT = \tau$, the wave power decreases to $e^{-4} \approx 1.8\%$ of the initial level. With the wave power observed by Van Allen Probes B and A at separated MLTs, we find that τ mainly fluctuates between 4 and 6 hr in the core frequency range of hiss waves (Figure 3d). The sudden enhancement (e.g., 11:40 UT) and reduction (e.g., 12:05 UT) of τ are related to the local density variation of Van Allen Probe B. In the source region, hiss waves tend to have higher power in the higher density region (Chen et al., 2012). After complicated propagation and substantial merging of rays with different initial conditions in the plasmasphere, the modulation characteristics have been smeared. As a result, when Van Allen Probe B in a low (high) density structure, we obtain a seemly enhanced (reduced) τ . Taking $\tau = 5$ hr, we estimate the duskside P_B to be $< 10^{-7}$ nT²/Hz, consistent with the ERG observations.

6. Discussion

The phenomenon described above appears to be not rare in the magnetosphere. During substorms, the enhanced magnetospheric electric field can cause a prompt erosion of the nightside plasmasphere (Su et al., 2018b) but a sunward drainage of the dayside plasmasphere (e.g., Goldstein et al., 2005). The substorm-injected electrons can access the dawn-to-noon plasmaspheric body and the noonside plasmaspheric plume and then internally generate hiss waves. During 06:00–08:00 UT on the same day (Figure S1 in the supporting information), Van Allen Probes also observed the plasmaspheric hiss with the frequency-drifting feature, albeit not as prominent as that during 11:00–13:00 UT (Figure 3). Because there was no signature of hot electron injection at the locations of both spacecraft, these waves were probably generated at larger L shells than Van Allen Probe A inside the plasmasphere. After 16:00 UT (Figures 1h and 1j), corresponding to the extremely weak and intermittent chorus in the prenoon sector (Van Allen Probe A), the moderate hiss occurred in the plasmaspheric body (Van Allen Probe B). We speculate that the hiss waves predominantly originated from the noonside plume (ERG) (Laakso et al., 2015; Su et al., 2018a), with little contribution from the plasmatrough chorus. Figures S2–S4 show the generation, propagation, and dissipation of frequency-drifting hiss once again observed by Van Allen Probes, GOES, and ERG missions on 2 December 2017. The 4 June 2014 event (Figure S5) is a good illustration of the substorm-enhanced plasmaspheric hiss with initially drifting lower cutoff frequency (70–200 Hz) and subsequently steady frequency coverage (> 200 Hz). The 7 November 2015 event (Figure S6) illustrates the generation of frequency-drifting hiss by substorm injection in the plasmaspheric plume. In all the events reported above, the drift of hiss lower cutoff was below 200 Hz, which can be explained by the frequency dependence of wave minimum resonant energy E_R (Summers et al., 2007). As shown in Figure S7, E_R varies steeply with f/f_{ce} in the low-frequency end but behaves smoothly in the high-frequency end. The frequency drift in the high-frequency range (> 200 Hz) would require a significant dispersive injection of electrons in a narrow energy range, which is hardly satisfied in the inner magnetosphere.

Recent studies (Chen et al., 2014; Li et al., 2013; Shi et al., 2017; Malaspina et al., 2017; Meredith et al., 2018) suggest that the internal linear instability is sufficient to explain the hiss waves at low frequencies (below ~ 200 Hz) and the external sources (chorus waves) are required for those waves at higher frequencies (from ~ 200 to $\sim 2,000$ Hz). Our observations indicate that the hiss waves in the frequency range from tens of hertz to several kilohertz can be generated locally inside the plasmasphere, probably through a combination of linear and nonlinear processes (Su et al., 2018a, 2018b). Previous statistical studies (Agapitov et al., 2018; Golden et al., 2012; Li et al., 2015; Meredith et al., 2004, 2018) have shown the asymmetrical distribution of hiss waves in MLT. Bortnik et al. (2008) and Chen et al. (2009) have provided an explanation for the hiss day-night asymmetry in the framework of “external origination” theory. Compared to the nightside region, the dayside region has a weaker damping effect on chorus waves and consequently stronger hiss waves. Here we suggest an alternative explanation for the asymmetrical distribution of hiss waves during substorms. Hot electrons directly inject into the dawn-to-noon plasmaspheric body and the noonside plasmaspheric plume and internally produce intense waves in the 6–14 MLT sector (Figure 2 of Meredith et al., 2018). Compared to the plasmaspheric body, the noonside plume-like structures extend to a larger radial distance and then have a greater chance to acquire the freshly injected electrons. The internally generated plume hiss waves are usually much stronger than those in the plasmaspheric body (Summers et al., 2008; Shi et al., 2019; Su et al., 2018a; Zhang et al., 2019). As a result, the statistically averaged hiss intensity peaks close to the noonside during substorms (Figure 2 of Meredith et al., 2018). The asymmetrical distribution of hiss waves is naturally attributed to the subsequent propagation and dissipation along both radial and azimuthal directions in the plasmasphere. The limited effective MLT coverage $\tau = 5$ hr reasonably explains the MLT asymmetry of hiss power in the previous statistical studies (Li et al., 2015; Meredith et al., 2018).

7. Summary

With the five spacecraft of Van Allen Probes, ERG, and GOES missions, we experimentally examine the generation, propagation, and dissipation of plasmaspheric hiss during substorms. The substorms injected hot electrons into the dawn-to-noon plasmaspheric sector and then produced the enhanced hiss waves from ~ 30 to $2,000$ Hz. The underlying generation mechanism of hiss waves was likely a combination of linear and nonlinear amplifications of ambient electromagnetic noise (Omura et al., 2015; Su et al., 2018a; Thorne et al., 1979). The energy dispersion of injected electrons caused the lower cutoff frequency of hiss waves to

rise slowly (70 Hz/hr). In the absence of high-resolution wave data, this long-lasting frequency drift feature served as a marker to trace the propagation of hiss waves over a large spatial scale. Because of resonant absorption by hot particles and leakage into the plasmatrough (Bortnik et al., 2008; Zhu et al., 2015), the hiss wave power was dissipated to $e^{-4} \approx 1.8\%$ of its original level approximately 5 hr MLT away from the source region in the dayside sector. Our results imply that the “internal origination” scenario is promising to explain the typical spectral and spatial distribution characteristics of substorm-enhanced plasmaspheric hiss waves. In future, more theoretical and statistical studies are required to evaluate the importance of internal origination scenario for the plasmaspheric hiss.

Acknowledgments

We acknowledge the entire Van Allen Probes, ERG, and GOES teams for the use of data. Van Allen Probes data were obtained from the websites <http://emfisis.physics.uiowa.edu/Flight/> for EMFISIS and <http://www.rbsp-ect.lanl.gov/data&urluscore;pub/> for ECT. GOES data were obtained online (from the website <https://cdaweb.sci.gsfc.nasa.gov/index.html/>). ERG (Arase) data were obtained from the ERG Science Center operated by ISAS/JAXA and ISEE/Nagoya University (<https://ergsc.isee.nagoya-u.ac.jp/index.shtml.en>; Miyoshi et al., 2018), with the specific data versions as follows: PWE/OFA L2 v02.01, PWE/HFA L3 v01, LEP-e L2 v02.02, MEP-e L2 v01.02, HEP L2 v02.00, MGF L2 v01.01, and OBT L2 v02. This work was supported by the National Natural Science Foundation of China Grants 41631071 and 41774170, the Chinese Academy of Sciences Grants KZCX2-EW-QN510 and KZZD-EW-01-4, the CAS Key Research Program of Frontier Sciences Grant QYZDB-SSW-DQC015, the National Key Basic Research Special Foundation of China Grant 2011CB811403, and the National Postdoctoral Program for Innovative Talents Grant BX20190310. Yoshizumi Miyoshi was supported by the Japan Society for the Promotion of Science Grants 15H05815 and 16H06286.

References

- Agapitov, O., Mourenas, D., Artemyev, A., Mozer, F. S., Bonnell, J. W., Angelopoulos, V., & Krasnoselskikh, V. (2018). Spatial extent and temporal correlation of chorus and hiss: Statistical results from multipoint THEMIS observations. *Journal of Geophysical Research: Space Physics*, 123, 8317–8330. <https://doi.org/10.1029/2018JA025725>
- Blake, J. B., Carranza, P. A., Claudepiere, S. G., Clemons, J. H., Crain, W. R., Dotan, Y., & Zakrzewski, M. P. (2013). The Magnetic Electron Ion Spectrometer (MagEIS) instruments aboard the Radiation Belt Storm Probes (RBSP) spacecraft. *Space Science Reviews*, 179, 383–421. <https://doi.org/10.1007/s11214-013-9991-8>
- Bortnik, J., Li, W., Thorne, R. M., Angelopoulos, V., Cully, C., Bonnell, J., & Roux, A. (2009). An observation linking the origin of plasmaspheric hiss to discrete chorus emissions. *Science*, 324, 775. <https://doi.org/10.1126/science.1171273>
- Bortnik, J., Thorne, R. M., & Meredith, N. P. (2008). The unexpected origin of plasmaspheric hiss from discrete chorus emissions. *Nature*, 452, 62–66. <https://doi.org/10.1038/nature06741>
- Breneman, A., Halford, A., Millan, R., McCarthy, M., Fennell, J., Sample, J., & Kletzing, C. (2015). Global-scale coherence modulation of radiation-belt electron loss from plasmaspheric hiss. *Nature*, 523, 193–195. <https://doi.org/10.1038/nature14515>
- Chen, L., Bortnik, J., Thorne, R. M., Horne, R. B., & Jordanova, V. K. (2009). Three-dimensional ray tracing of VLF waves in a magnetospheric environment containing a plasmaspheric plume. *Geophysical Research Letters*, 36, 22101. <https://doi.org/10.1029/2009GL040451>
- Chen, L., Li, W., Bortnik, J., & Thorne, R. M. (2012). Amplification of whistler-mode hiss inside the plasmasphere. *Geophysical Research Letters*, 39, 8111. <https://doi.org/10.1029/2012GL051488>
- Chen, L., Thorne, R. M., Bortnik, J., Li, W., Horne, R. B., Reeves, G. D., & Fennell, J. F. (2014). Generation of unusually low frequency plasmaspheric hiss. *Geophysical Research Letters*, 41, 5702–5709. <https://doi.org/10.1002/2014GL060628>
- Chen, L., Thorne, R. M., Li, W., Bortnik, J., Turner, D., & Angelopoulos, V. (2012). Modulation of plasmaspheric hiss intensity by thermal plasma density structure. *Geophysical Research Letters*, 39, 14103. <https://doi.org/10.1029/2012GL052308>
- Chum, J., & Santolík, O. (2005). Propagation of whistler-mode chorus to low altitudes: Divergent ray trajectories and ground accessibility. *Annales Geophysicae*, 23, 3727–3738. <https://doi.org/10.5194/angeo-23-3727-2005>
- Church, S. R., & Thorne, R. M. (1983). On the origin of plasmaspheric hiss—Ray path integrated amplification. *Journal of Geophysical Research*, 88, 7941–7957. <https://doi.org/10.1029/JA088iA10p07941>
- Davis, G. K. (2007). History of the NOAA satellite program. *Journal of Applied Remote Sensing*, 1(1), 12504.
- Denton, R. E., Goldstein, J., & Menietti, J. D. (2002). Field line dependence of magnetospheric electron density. *Geophysical Research Letters*, 29(24), 2205. <https://doi.org/10.1029/2002GL015963>
- Denton, R. E., Goldstein, J., Menietti, J. D., & Young, S. L. (2002). Magnetospheric electron density model inferred from Polar plasma wave data. *Journal of Geophysical Research*, 107, 1386. <https://doi.org/10.1029/2001JA009136>
- Funsten, H. O., Skoug, R. M., Guthrie, A. A., MacDonald, E. A., Baldonado, J. R., Harper, R. W., & Chen, J. (2013). Helium, Oxygen, Proton, and Electron (HOPE) mass spectrometer for the Radiation Belt Storm Probes mission. *Space Science Reviews*, 179, 423–484. <https://doi.org/10.1007/s11214-013-9968-7>
- GOES N Series Data Book (2009). Revision C. Boeing Satellite Systems Inc.
- Golden, D. I., Spasojevic, M., Li, W., & Nishimura, Y. (2012). Statistical modeling of plasmaspheric hiss amplitude using solar wind measurements and geomagnetic indices. *Geophysical Research Letters*, 39, 6103. <https://doi.org/10.1029/2012GL051185>
- Goldstein, J., Sandel, B. R., Forrester, W. T., Thomsen, M. F., & Hairston, M. R. (2005). Global plasmasphere evolution 22–23 April 2001. *Journal of Geophysical Research: Space Physics*, 110, A12218. <https://doi.org/10.1029/2005JA011282>
- Green, J. L., Boardsen, S., Garcia, L., Taylor, W. W. L., Fung, S. F., & Reinisch, B. W. (2005). On the origin of whistler mode radiation in the plasmasphere. *Journal of Geophysical Research*, 110, A03201. <https://doi.org/10.1029/2004JA010495>
- Hartley, D. P., Kletzing, C. A., Kurth, W. S., Bounds, S. R., Averkamp, T. F., Hospodarsky, G. B., & Watt, C. E. J. (2016). Using the cold plasma dispersion relation and whistler mode waves to quantify the antenna sheath impedance of the Van Allen Probes EFW instrument. *Journal of Geophysical Research: Space Physics*, 121, 4590–4606. <https://doi.org/10.1002/2016JA022501>
- Horne, R. B. (1989). Path-integrated growth of electrostatic waves: The generation of terrestrial myriametric radiation. *Journal of Geophysical Research*, 94, 8895. <https://doi.org/10.1029/JA094iA07p08895>
- Kasahara, Y., Kasaba, Y., Kojima, H., Yagitani, S., Ishisaka, K., Kumamoto, A., & Shinohara, I. (2018). The Plasma Wave Experiment (PWE) on board the Arase (ERG) satellite. *Earth, Planets and Space*, 70(1), 86. <https://doi.org/10.1186/s40623-018-0842-4>
- Kasahara, S., Yokota, S., Mitani, T., Asamura, K., Hirahara, M., Shibano, Y., & Takashima, T. (2018). Medium-energy particle experiments—Electron analyzer (MEP-e) for the Exploration of energization and Radiation in Geospace (ERG) mission. *Earth, Planets, and Space*, 70, 69. <https://doi.org/10.1186/s40623-018-0847-z>
- Kazama, Y., Wang, B. J., Wang, S. Y., Ho, P. T. P., Tam, S. W. Y., Chang, T. F., & Asamura, K. (2017). Low-energy particle experiments—Electron analyzer (LEPe) onboard the Arase spacecraft. *Earth, Planets, and Space*, 69, 165. <https://doi.org/10.1186/s40623-017-0748-6>
- Kennel, C. (1966). Low-frequency whistler mode. *Physics of Fluids*, 9, 2190–2202. <https://doi.org/10.1063/1.1761588>
- Kletzing, C. A., Kurth, W. S., Acuna, M., MacDowall, R. J., Torbert, R. B., Averkamp, T., & Tyler, J. (2013). The Electric and Magnetic Field Instrument Suite and Integrated Science (EMFISIS) on RBSP. *Space Science Review*, 179, 127–181. <https://doi.org/10.1007/s11214-013-9993-6>

- Kumamoto, A., Tsuchiya, F., Kasahara, Y., Kasaba, Y., Kojima, H., Yagitani, S., & Obara, T. (2018). High Frequency Analyzer (HFA) of Plasma Wave Experiment (PWE) onboard the Arase spacecraft. *Earth, Planets, and Space*, 70(1), 82. <https://doi.org/10.1186/s40623-018-0854-0>
- Kurth, W. S., Pascuale, S. D., Faden, J. B., Kletzing, C. A., Hospodarsky, G. B., Thaller, S., & Wygant, J. R. (2014). Electron densities inferred from plasma wave spectra obtained by the Waves instrument on Van Allen Probes. *Journal of Geophysical Research: Space Physics*, 120, 904–914. <https://doi.org/10.1002/2014JA020857>
- Laakso, H., Santolik, O., Horne, R., Kolmasová, I., Escoubet, P., Masson, A., & Taylor, M. (2015). Identifying the source region of plasmaspheric hiss. *Geophysical Research Letters*, 42, 3141–3149. <https://doi.org/10.1002/2015GL063755>
- Li, W., Chen, L., Bortnik, J., Thorne, R. M., Angelopoulos, V., Kletzing, C. A., & Hospodarsky, G. B. (2015). First evidence for chorus at a large geocentric distance as a source of plasmaspheric hiss: Coordinated THEMIS and Van Allen Probes observation. *Geophysical Research Letters*, 42, 241–248. <https://doi.org/10.1002/2014GL062832>
- Li, W., Ma, Q., Thorne, R. M., Bortnik, J., Kletzing, C. A., Kurth, W. S., & Nishimura, Y. (2015). Statistical properties of plasmaspheric hiss derived from Van Allen Probes data and their effects on radiation belt electron dynamics. *Journal of Geophysical Research: Space Physics*, 120, 3393–3405. <https://doi.org/10.1002/2015JA021048>
- Li, W., Thorne, R. M., Bortnik, J., Reeves, G. D., Kletzing, C. A., Kurth, W. S., & Thaller, S. A. (2013). An unusual enhancement of low-frequency plasmaspheric hiss in the outer plasmasphere associated with substorm-injected electrons. *Geophysical Research Letters*, 40, 3798–3803. <https://doi.org/10.1002/grl.50787>
- Liu, N., Su, Z., Gao, Z., Zheng, H., Wang, Y., & Wang, S. (2019). Magnetospheric chorus, exohiss, and magnetosonic emissions simultaneously modulated by fundamental toroidal standing Alfvén waves following solar wind dynamic pressure fluctuations. *Geophysical Research Letters*, 46, 1900–1910. <https://doi.org/10.1029/2018GL081500>
- Liu, N., Su, Z., Gao, Z., Zheng, H., Wang, Y., Wang, S., & Wygant, J. R. (2017). Simultaneous disappearances of plasmaspheric hiss, exohiss, and chorus waves triggered by a sudden decrease in solar wind dynamic pressure. *Geophysical Research Letters*, 44, 52–61. <https://doi.org/10.1002/2016GL071987>
- Liu, N., Su, Z., Zheng, H., Wang, Y., & Wang, S. (2018). Magnetosonic harmonic falling and rising frequency emissions potentially generated by nonlinear wave-wave interactions in the Van Allen radiation belts. *Geophysical Research Letters*, 45, 7985–7995. <https://doi.org/10.1029/2018GL079232>
- Liu, N., Su, Z., Zheng, H., Wang, Y., & Wang, S. (2018). Prompt disappearance and emergence of radiation belt magnetosonic waves induced by solar wind dynamic pressure variations. *Geophysical Research Letters*, 45, 585–594. <https://doi.org/10.1002/2017GL076382>
- Lyons, L. R., Thorne, R. M., & Kennel, C. F. (1972). Pitch-angle diffusion of radiation belt electrons within the plasmasphere. *Journal of Geophysical Research*, 77, 3455–3474. <https://doi.org/10.1029/JA077i019p03455>
- Malaspina, D. M., Jaynes, A. N., Boulé, C., Bortnik, J., Thaller, S. A., Ergun, R. E., & Wygant, J. R. (2016). The distribution of plasmaspheric hiss wave power with respect to plasmapause location. *Geophysical Research Letters*, 43, 7878–7886. <https://doi.org/10.1002/2016GL069982>
- Malaspina, D. M., Jaynes, A. N., Hospodarsky, G., Bortnik, J., Ergun, R. E., & Wygant, J. (2017). Statistical properties of low-frequency plasmaspheric hiss. *Journal of Geophysical Research: Space Physics*, 122, 8340–8352. <https://doi.org/10.1002/2017JA024328>
- Matsuda, S., Kasahara, Y., Kojima, H., Kasaba, Y., Yagitani, S., Ozaki, M., & Shinohara, I. (2018). Onboard software of Plasma Wave Experiment aboard Arase: Instrument management and signal processing of Waveform Capture/Onboard Frequency Analyzer. *Earth, Planets, and Space*, 70(1), 75. <https://doi.org/10.1186/s40623-018-0838-0>
- Matsuoka, A., Teramoto, M., Nomura, R., Nosé, M., Fujimoto, A., Tanaka, Y., & Shinohara, I. (2018). The ARASE (ERG) magnetic field investigation. *Earth, Planets, and Space*, 70(1), 43. <https://doi.org/10.1186/s40623-018-0800-1>
- Mauk, B. H., Fox, N. J., Kanekal, S. G., Kessel, R. L., Sibeck, D. G., & Ukhorskiy, A. (2013). Science objectives and rationale for the Radiation Belt Storm Probes Mission. *Space Science Review*, 179, 3–27. <https://doi.org/10.1007/s11214-012-9908-y>
- Meredith, N. P., Horne, R. B., Clilverd, M. A., Horsfall, D., Thorne, R. M., & Anderson, R. R. (2006). Origins of plasmaspheric hiss. *Journal of Geophysical Research*, 111, 9217. <https://doi.org/10.1029/2006JA011707>
- Meredith, N. P., Horne, R. B., Kersten, T., Li, W., Bortnik, J., Sicard, A., & Yearby, K. H. (2018). Global model of plasmaspheric hiss from multiple satellite observations. *Journal of Geophysical Research: Space Physics*, 123, 4526–4541. <https://doi.org/10.1029/2018JA025226>
- Meredith, N. P., Horne, R. B., Thorne, R. M., Summers, D., & Anderson, R. R. (2004). Substorm dependence of plasmaspheric hiss. *Journal of Geophysical Research*, 109, A06209. <https://doi.org/10.1029/2004JA010387>
- Mitani, T., Takashima, T., Kasahara, S., Miyake, W., & Hirahara, M. (2018). High-energy electron experiments (HEP) aboard the ERG (Arase) satellite. *Earth, Planets, and Space*, 70, 77. <https://doi.org/10.1186/s40623-018-0853-1>
- Miyoshi, Y., Hori, T., Shoji, M., Teramoto, M., Chang, T. F., Segawa, T., & Shinohara, I. (2018). The ERG Science Center. *Earth, Planets, and Space*, 70(1), 96. <https://doi.org/10.1186/s40623-018-0867-8>
- Miyoshi, Y., Shinohara, I., Takashima, T., Asamura, K., Higashio, N., Mitani, T., & Seki, K. (2018). Geospace exploration project ERG. *Earth, Planets, and Space*, 70(1), 101. <https://doi.org/10.1186/s40623-018-0862-0>
- Mourenas, D., Ma, Q., Artemyev, A. V., & Li, W. (2017). Scaling laws for the inner structure of the radiation belts. *Geophysical Research Letters*, 44, 3009–3018. <https://doi.org/10.1002/2017GL072987>
- Nakamura, S., Omura, Y., & Summers, D. (2018). Fine structure of whistler mode hiss in plasmaspheric plumes observed by the Van Allen Probes. *Journal of Geophysical Research: Space Physics*, 123, 9055–9064. <https://doi.org/10.1029/2018JA025803>
- Nakamura, S., Omura, Y., Summers, D., & Kletzing, C. A. (2016). Observational evidence of the nonlinear wave growth theory of plasmaspheric hiss. *Geophysical Research Letters*, 43, 10. <https://doi.org/10.1002/2016GL070333>
- Omura, Y., Katoh, Y., & Summers, D. (2008). Theory and simulation of the generation of whistler-mode chorus. *Journal of Geophysical Research*, 113, 4223. <https://doi.org/10.1029/2007JA012622>
- Omura, Y., Nakamura, S., Kletzing, C. A., Summers, D., & Hikishima, M. (2015). Nonlinear wave growth theory of coherent hiss emissions in the plasmasphere. *Journal of Geophysical Research: Space Physics*, 120, 7642–7657. <https://doi.org/10.1002/2015JA021520>
- Russell, C. T., Holzer, R. E., & Smith, E. J. (1969). OGO 3 observations of ELF noise in the magnetosphere. 1. Spatial extent and frequency of occurrence. *Journal of Geophysical Research*, 74, 755–777. <https://doi.org/10.1029/JA074i003p00755>
- Santolik, O., Pickett, J. S., Gurnett, D. A., Menietti, J. D., Tsurutani, B. T., & Verkhoglyadova, O. (2010). Survey of Poynting flux of whistler mode chorus in the outer zone. *Journal of Geophysical Research*, 115, A00F13. <https://doi.org/10.1029/2009JA014925>
- Santolik, O., Parrot, M., & Lefevre, F. (2003). Singular value decomposition methods for wave propagation analysis. *Radio Science*, 38, 1010. <https://doi.org/10.1029/2000RS002523>
- Santolik, O., Pickett, J. S., Gurnett, D. A., & Storey, L. R. O. (2002). Magnetic component of narrowband ion cyclotron waves in the auroral zone. *Journal of Geophysical Research*, 107, 1444. <https://doi.org/10.1029/2001JA000146>

- Shi, R., Li, W., Ma, Q., Green, A., Kletzing, C. A., Kurth, W. S., & Reeves, G. D. (2019). Properties of whistler mode waves in Earth's plasmasphere and plumes. *Journal of Geophysical Research: Space Physics*, 124, 1035–1051. <https://doi.org/10.1029/2018JA026041>
- Shi, R., Li, W., Ma, Q., Reeves, G. D., Kletzing, C. A., Kurth, W. S., & Claudepierre, S. G. (2017). Systematic evaluation of low-frequency hiss and energetic electron injections. *Journal of Geophysical Research: Space Physics*, 122, 10,263–10,274. <https://doi.org/10.1002/2017JA024571>
- Sonwalkar, V. S., & Inan, U. S. (1989). Lightning as an embryonic source of VLF hiss. *Journal of Geophysical Research*, 94, 6986–6994. <https://doi.org/10.1029/JA094iA06p06986>
- Spence, H. E., Reeves, G. D., Baker, D. N., Blake, J. B., Bolton, M., Bourdarie, S., & Thorne, R. M. (2013). Science goals and overview of the Energetic Particle, Composition, and Thermal Plasma (ECT) suite on NASAs Radiation Belt Storm Probes (RBSP) mission. *Space Science Review*, 179, 311–336. <https://doi.org/10.1007/s11214-013-0007-5>
- Su, Z., Liu, N., Zheng, H., Wang, Y., & Wang, S. (2018a). Large-amplitude extremely low frequency hiss waves in plasmaspheric plumes. *Geophysical Research Letters*, 45, 565–577. <https://doi.org/10.1002/2017GL076754>
- Su, Z., Liu, N., Zheng, H., Wang, Y., & Wang, S. (2018b). Multipoint observations of nightside plasmaspheric hiss generated by substorm-injected electrons. *Geophysical Research Letters*, 45, 10. <https://doi.org/10.1029/2018GL079927>
- Su, Z., Zhu, H., Xiao, F., Zheng, H., Wang, Y., Shen, C., & Wygant, J. R. (2015). Disappearance of plasmaspheric hiss following interplanetary shock. *Geophysical Research Letters*, 42, 3129–3140. <https://doi.org/10.1002/2015GL063906>
- Summers, D., Ni, B., & Meredith, N. P. (2007). Timescales for radiation belt electron acceleration and loss due to resonant wave-particle interactions: 1. Theory. *Journal of Geophysical Research*, 112, A04206. <https://doi.org/10.1029/2006JA011801>
- Summers, D., Ni, B., & Meredith, N. P. (2007). Timescales for radiation belt electron acceleration and loss due to resonant wave-particle interactions: 2. Evaluation for VLF chorus, ELF hiss, and electromagnetic ion cyclotron waves. *Journal of Geophysical Research*, 112, A04207. <https://doi.org/10.1029/2006JA011993>
- Summers, D., Ni, B., Meredith, N. P., Horne, R. B., Thorne, R. M., Moldwin, M. B., & Anderson, R. R. (2008). Electron scattering by whistler-mode ELF hiss in plasmaspheric plumes. *Journal of Geophysical Research*, 113, A04219. <https://doi.org/10.1029/2007JA012678>
- Summers, D., Omura, Y., Nakamura, S., & Kletzing, C. A. (2014). Fine structure of plasmaspheric hiss. *Journal of Geophysical Research: Space Physics*, 119, 9134–9149. <https://doi.org/10.1002/2014JA020437>
- Thorne, R. M., Church, S. R., & Gorney, D. J. (1979). On the origin of plasmaspheric hiss—The importance of wave propagation and the plasmapause. *Journal of Geophysical Research*, 84, 5241–5247. <https://doi.org/10.1029/JA084iA09p05241>
- Thorne, R. M., Li, W., Ni, B., Ma, Q., Bortnik, J., Baker, D. N., et al. (2013). Evolution and slow decay of an unusual narrow ring of relativistic electrons near $L \sim 3.2$ following the September 2012 magnetic storm. *Geophysical Research Letters*, 40, 3507–3511. <https://doi.org/10.1002/grl.50627>
- Thorne, R. M., Smith, E. J., Burton, R. K., & Holzer, R. E. (1973). Plasmaspheric hiss. *Journal of Geophysical Research*, 78, 1581–1596. <https://doi.org/10.1029/JA078i010p01581>
- Tsurutani, B. T., Falkowski, B. J., Pickett, J. S., Santolik, O., & Lakhina, G. S. (2015). Plasmaspheric hiss properties: Observations from Polar. *Journal of Geophysical Research: Space Physics*, 120, 414–431. <https://doi.org/10.1002/2014JA020518>
- Tsurutani, B. T., Falkowski, B. J., Verkhoglyadova, O. P., Pickett, J. S., Santolik, O., & Lakhina, G. S. (2012). Dayside ELF electromagnetic wave survey: A Polar statistical study of chorus and hiss. *Journal of Geophysical Research*, 117, A00L12. <https://doi.org/10.1029/2011JA017180>
- Tsurutani, B. T., Smith, E. J., & Thorne, R. M. (1975). Electromagnetic hiss and relativistic electron losses in the inner zone. *Journal of Geophysical Research*, 80, 600–607. <https://doi.org/10.1029/JA080i004p00600>
- Tsyganenko, N. A., & Sitnov, M. I. (2005). Modeling the dynamics of the inner magnetosphere during strong geomagnetic storms. *Journal of Geophysical Research*, 110, A03208. <https://doi.org/10.1029/2004JA010798>
- Zhang, W., Ni, B., Huang, H., Summers, D., Fu, S., Xiang, Z., & Hua, M. (2019). Statistical properties of hiss in plasmaspheric plumes and associated scattering losses of radiation belt electrons. *Geophysical Research Letters*, 46, 5670–5680. <https://doi.org/10.1029/2018GL081863>
- Zhu, H., Su, Z., Xiao, F., Zheng, H., Wang, Y., Shen, C., et al. (2015). Plasmatrough exohiss waves observed by Van Allen Probes: Evidence for leakage from plasmasphere and resonant scattering of radiation belt electrons. *Geophysical Research Letters*, 42, 1012–1019. <https://doi.org/10.1002/2014GL062964>